Torabnia et al. International Journal of Mechanical and Materials Engineering (2019) 14:16
https://doi.org/10.1186/s40712-019-0112-7

International Journal of Mechanical and Materials Engineering

ORIGINAL PAPER Open Access

An analytical investigation of elastic-plastic deformation of FGM hollow rotors under a high centrifugal effect

Shams Torabnia[1*], Sepideh Aghajani[2] and Mohammadreza Hemati[2]

Abstract

Functionally graded material shafts are the main part of many modern rotary machines such as turbines and electric motors. The purpose of this study is to present an analytical solution of the elastic-plastic deformation of functionally graded material hollow rotor under a high centrifugal effect and finally determine the maximum allowed angular velocity of a hollow functionally graded material rotating shaft. Introducing non-dimensional parameters, the equilibrium equation has been analytically solved. The results for variable material properties are compared with the homogeneous rotor and the case in which Young's modulus is the only variable while density and yield stress are considered to be constant. It is shown that material variation has a considerable effect on the stress and strain components and radial displacement. Considering variable density and yield stress causes yielding onset from inner, outer, or simultaneously from both inner and outer rotor shaft radius in contrast to earlier researches that modulus of elasticity was the only variable. The effects of the density on the failure of a functionally graded material elastic fully plastic in a hollow rotating shaft are investigated for the first time in this study with regard to Tresca's yield criterial. Numerical simulations are used to verify the derived formulations which are in satisfying agreement.

Keywords: Functionally graded material, Hollow shaft, Elastic-plastic analysis, Angular velocity, Plane strain

Introduction

Functionally graded materials (FGM) are finding vast applications in different rotary systems such as DC motors with a magnetic membrane and chemical resistant hydraulic motors (Mahamood & Akinlabi, 2017), gas turbine rotors (Bahaloo, Papadopolus, & Ghosha, 2016; Klocke, Klink, & Veselovac, 2014; Lal, Jagtap, & Singh, 2013), and modern vehicle drive train systems (Kaviprakash, Kannan, Lawrence, & Regan, 2014; Lee, Kim, Kim, & Kim, 2004; Moorthy, Mitiku, & Sridhar, 2013). Computing different stresses and the radial displacement of FGM rotors are required to determine the maximum allowed angular velocity (Nino, Hirai, & Watanabe, 1987). Timoshenko (Timoshenko & Goodier, 1970), Mendelson (Mendelson, 1968), Chakrabarty (Chakrabarty, 2006) and Mack (Mack, 1991) analyzed a homogenous rotor. You analyzed a rotating FGM disk (You, You, Zhang, & Li, 2007) and Dai considered the magnetic properties of the FGM disk (Dai & Dai, 2017). Fukui and Yamanaka studied elastic analysis for thick-walled FGM tubes subjected to internal pressure (Fukui & Yamanaka, 1991). Figueiredo studied FGM pipes (Figueiredo, Borges, & Rochinha, 2008). Tutunku and Ozturk determined solutions for stresses in FGM pressure vessels (Tutuncu & Ozturk, 2001). Jabbari (Jabbari, Sohrabpour, & Eslami, 2002) and Ansari (AnsariSadrabadi et al., 2017) investigated mechanical and thermal stresses in an FGM hollow cylinder under symmetric loads. You considered an FGM pressurized sphere with a nonlinear variable modulus of elasticity in a radial direction (You, Zhang, & You, 2005). Dai et al. studied a pressurized magneto elastic FGM tube (Dai, Fu, & Dong, 2006). Hosseini et al. analyzed the thermo-elastic behavior of an FG rotating disk (HosseiniKordkheili & Naghdabadi, 2006). Duc (Duc, Lee, Nguyen-Thoi, & Thang, 2017; Duc, Thang, Dao, & Vantac, 2015), Khoa (Khoa, Thiem, Thiem, & Duc, 2019), and El-Haina (El-Haina, Bakora, Bousahla, Tounsi, & Mahmoud, 2017) considered the buckling problem in their research.

* Correspondence: shams.torabnia@gmail.com
[1]Sharif University of Technology, Azadi St., Tehran, Iran
Full list of author information is available at the end of the article

Thom (Thom, Kien, Duc, Duc, & Tinh, 2017) analyzed a two-dimensional analysis on an FGM plane by plane strain theories. Eraslan (Eraslan & Akis, 2006a) gave an analytical solution for rotating disks and tubes in plane stress and plane strain state, and studied stress solutions of FGM shafts and disks (Eraslan & Akis, 2006b; Eraslan & Akis, 2006c). Kargarnovin et al. (Kargarnovin, Faghidian, & Arghavani, 2007) investigated FGM circular plates with arbitrary rotational symmetric load. Akis (Akis & Eraslan, 2007) studied a rotating FGM shaft problem in the elastic-plastic state of stress with a variable modulus of elasticity. Tsiatas (Tsiatas & Babouskos, 2017) worked on torsional FGM bar. Akis studied the elasticity solution for thick-walled FG spherical pressure vessels with linearly and exponentially varying properties (Akis, 2009). ZamaniNejad and Rahimi studied the elasticity of an FGM rotating cylindrical pressure vessels (ZamaniNejad & Rahimi, 2010). Peng and Li investigated an orthotropic hollow rotating disk with a variable modulus of elasticity and density (Peng & Li, 2012). Some others studied creep for FGM material under thermal condition (Bose & Rattan, 2018; Khanna, Gupta, & Nigam, 2017; Zharfi & Ekhteraei-Toussi, 2018). Yildirim (Yildirim & Tutuncu, 2018), Seraj (Seraj & Ganesan, 2018), Bahaadini (Bahaadini & Saidi, 2018), Swaminathan (Swaminathan, Naveenkumar, Zenkour, & Carrera, 2015), Duc (Duc, 2013; Duc & Cong, 2018; Duc, Homayoun, Quan, & Khoa, 2019; Duc, Nguyen, & Khoa, 2017; Duc, Tran, & Cong, 2016), and Bouderba (Bouderba, Houari, Tounsi, & Mahmoud, 2016) worked on rotor instabilities and vibrations under different conditions. Burzyński (Burzyński, Chróścielewski, Daszkiewicz, & Witkowski, 2018) worked on a FEM method to understand elasto-plastic behaviors of FGM shells, and Mathew (Mathew, Natarajan, & Pañeda, 2018) considered size effects in his researches. Duc (Duc, 2016a; Duc, 2016b; Duc et al., 2015; Duc, Bich, & Cong, 2016; Duc, Khoa, & Thiem, 2018; Duc, Kim, & Chan, 2018; Duc, Thuy Anh, & Cong, 2014) specifically studied thermal effects such as buckling, thermal instability, and dynamic thermal loads circular sections. The authors (Torabnia, Hemati, & Aghajanib, 2019) considered the elastic behavior of a hollow FGM rotor.

Although the previous studies are valuable, none of them considered the plastic effects in an analytical model. All previous jobs used a numerical method such as FEM to solve the plastic model. In the present work, the analysis is based on small deformation theory. The shaft is assumed to be infinitely long (plane strain). The maximum allowed angular velocity has been defined as the angular velocity in which yielding initiates based on Tresca's criterion. Non-dimensional parameters are introduced based on the geometry and material parameters. Stress components are derived using generalized Hook's law. To identify the stress components ordering, non-dimensional stress components are plotted for the special case of equal exponent parameters with the variable radius ratio. The results show when the exponent parameters vary between − 2 and 2, hoop stress and radial stress components are the largest and the smallest stress components. The effect of variation of density and yield stress is investigated on the maximum allowed angular velocity and has a considerable effect on the stress distribution and yielding initiation and the maximum allowed angular velocity. For the first time, density variation is considered with variable density and radius ratio of a hollow rotor on elastic and plastic behavior and maximum allowed angular velocity are discussed (Fig. 1).

Methods/experimental

In this section, the aims and methodology of the study presented by an explanation of the governing equations of a hollow rotor with variable properties through its geometry. Material properties in an FGM may vary in any direction. Here, modulus of elasticity, density, and yield stress are functions of radial dimension:

$$E(r) = E_0(r/b)^{n_E}, \rho(r) = \rho_0(r/b)^{n_\rho}, \sigma_Y(r) = \sigma_0(r/b)^{n_\sigma} \quad (1)$$

The material properties modeled with the power-law function. Different exponent parameters allow various shapes for material variation. By formulating in the cylindrical coordinate system (r, θ, z) for an infinitely long tube which rotates about longitude axis (Timoshenko & Goodier, 1970):

$$\frac{d}{dr}(r\sigma_r) - \sigma_\theta = -\rho r^2 \omega^2 \quad (2)$$

The strain and radial displacement relation is:

$$\varepsilon_r = du(r)/dr, \varepsilon_\theta = u(r)/r \quad (3)$$

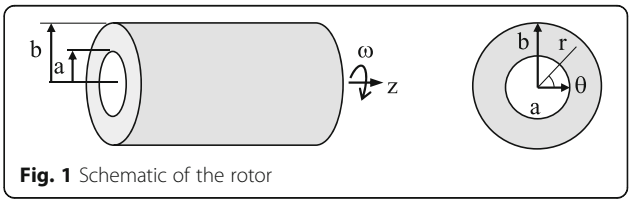

Fig. 1 Schematic of the rotor

Plane strain condition is due to a long tube which causes the zero value for the longitude strain. Manipulating stress-strain and radial displacement:

$$\begin{aligned}\sigma_r &= \frac{E}{(1+\nu)(1-2\nu)}\left((1-\nu)\frac{du(r)}{dr}+\nu\frac{u(r)}{r}\right), \sigma_\theta \\ &= \frac{E}{(1+\nu)(1-2\nu)}\left((1-\nu)\frac{u(r)}{r}+\nu\frac{du(r)}{dr}\right), \sigma_z \\ &= \nu(\sigma_r+\sigma_\theta)\end{aligned} \tag{4}$$

Substituting (4) into (2) in elastic region:

$$\begin{aligned}&r^2\frac{d^2}{dr^2}u(r) \\ &+(1+n_E)r\left(\frac{d}{dr}u(r)\right)-\frac{1-\nu(1+n_E)}{1-\nu}u(r) \\ &=-\frac{(1+\nu)(1-2\nu)\rho_0\omega^2}{(1-\nu)E_0}b^{(n_E-n\rho)}r^{(3+n\rho-n_E)}\end{aligned} \tag{5}$$

The general reformed solution of (5) is:

$$\overline{u}(\overline{r}) = C_1\overline{r}^{\left(\frac{-n_E-k}{2}\right)}+C_2\overline{r}^{\left(\frac{-n_E+k}{2}\right)}-A_1\overline{\omega}^2\overline{r}^{(n\rho-n_E+3)} \tag{6}$$

A solution of (6) is simplified and taken into a non-dimensional form to be independent of material properties. Non-dimensional quantities are presented:

$$\begin{aligned}&\overline{r}=r/b, \overline{h}=a/b, \overline{u}=u/b, \overline{\omega}^2=\rho_0\omega^2b^2/E_0 \\ &k=\frac{\sqrt{n_E{}^2-2n_E{}^2\nu+\nu^2n_E{}^2+4-8\nu+4\nu^2-4\nu n_E+4\nu^2n_E}}{1-\nu} \\ &A_1=\frac{2\nu^2+\nu-1}{(4+n_\rho)(n_\rho-n_E+2)\nu-n_\rho{}^2+(n_E-6)n_\rho-8+3n_E}\end{aligned} \tag{7}$$

ω defined as the non-dimensional rotating velocity. Substituting radial displacement into (5):

$$\begin{aligned}\overline{\sigma}_r &= \frac{\overline{r}^{n_E}}{(1+\nu)(1-2\nu)}\left\{\begin{array}{l}\nu\left(C_1\overline{r}^{m_1}+C_2\overline{r}^{m_2}-A_1\overline{\omega}^2\overline{r}^{\left(2+n_\rho-n_E\right)}\right)+ \\ (1-\nu)\left(\begin{array}{l}C_1\overline{r}^{m_1}\frac{(-n_E-k)}{2}+C_2\overline{r}^{m_2}\frac{(-n_E+k)}{2} \\ -A_1\overline{\omega}^2(3+n_\rho-n_E)\overline{r}(2+n_\rho-n_E)\end{array}\right)\end{array}\right\} \\ \overline{\sigma}_\theta &= \frac{\overline{r}^{n_E}}{(1+\nu)(1-2\nu)}\left\{\begin{array}{l}(1-\nu)\left(C_1\overline{r}^{m_1}+C_2\overline{r}^{m_2}-A_1\overline{\omega}^2\overline{r}^{\left(2+n_\rho-n_E\right)}\right)+ \\ \nu\left(\begin{array}{l}C_1\overline{r}^{m_1}\frac{(-n_E-k)}{2}+C_2\overline{r}^{m_2}\frac{(-n_E+k)}{2} \\ -A_1\overline{\omega}^2(3+n_\rho-n_E)\overline{r}^{\left(2+n_\rho-n_E\right)}\end{array}\right)\end{array}\right\} \\ \overline{\sigma}_z &= \frac{\nu\times\overline{r}^{n_E}}{(1+\nu)(1-2\nu)}\left\{C_1\overline{r}^{m_1}m_3+C_2\overline{r}^{m_2}m_4-A_1\overline{\omega}^2\overline{r}^{\left(2+n_\rho-n_E\right)}(4+n_\rho-n_E)\right\}\end{aligned} \tag{8}$$

σi stands for non-dimensional stress which is defined in the form σi = σi/E0. The constants used in (8) are:

$$\begin{aligned}m_1 &= \frac{-n_E-k-2}{2}, m_2=\frac{-n_E+k-2}{2}, m_3 \\ &= \frac{-n_E-k+2}{2}, m_4=\frac{-n_E+k+2}{2}\end{aligned} \tag{9}$$

To obtain C_1 and C_2 in radial displacement (7), two boundary conditions are needed. Since no pressure is applied to the inner and outer surfaces of the rotor, the boundary conditions are considered as σ_Y(r=h) = 0 & σ_Y(r=1) = 0. Constants C_1 and C_2 are:

$$C_1=-2A_1A_2\bar{\omega}^2\frac{\left[\bar{h}^{n_\rho+4}-\bar{h}^{-m_1}\right]}{\left(\bar{h}^{-m_1}-\bar{h}^{-m_2}\right)}, C_2=-2A_1A_3\bar{\omega}^2\frac{\left[\bar{h}^{n_\rho+4}-\bar{h}^{-m_2}\right]}{\left(\bar{h}^{-m_1}-\bar{h}^{-m_2}\right)} \tag{10}$$

For A_2 and A_3:

$$\begin{aligned}A_2 &= \frac{3-\nu n_\rho+\nu n_E-2\nu+n_\rho-n_E}{-n_E-k+\nu n_E+\nu k+2\nu}, A_3 \\ &= \frac{3-\nu n_\rho+\nu n_E-2\nu+n_\rho-n_E}{-2\nu-\nu n_E-k+n_E+\nu k}\end{aligned} \tag{11}$$

Tresca's criterion is considered to determine yield condition and allowed the angular velocity of the shaft. As the results show, yielding is a function of exponent parameters of material variables (n_E, n_ρ, n_σ). In this paper, the results are discussed on the equality of the exponents of material variables. According to Fig. 3 for the state of equal exponents in the range of $-2 \le n_i \le 2$ and $0.5 \le h \le 1$, the stress components have the order of $\sigma_\theta \ge \sigma_z \ge \sigma_r$. The yield criterion is in the form of $\sigma\theta-\sigma_r = \sigma_Y$. Rearranging into a non-dimensional form gives:

$$\overline{\sigma}_\theta-\overline{\sigma}_{\overline{r}}=\frac{\sigma_0}{E_0}\overline{r}^{n_\sigma}=\sigma_0\overline{r}^{n_\sigma}\Rightarrow\overline{\sigma}_{\text{Tresca}}=\frac{(\overline{\sigma}_\theta-\overline{\sigma}_{\overline{r}})}{\overline{\sigma}_0}-\overline{r}n_\sigma \tag{12}$$

By substituting hoop and radial stresses in the yield's criterion following equation formed.

$$\bar{\sigma}_{\text{Tresca}}=\frac{\bar{\omega}^2A_1\bar{r}^{n_E}}{(1+\nu)\bar{\sigma}_0}\left\{\begin{array}{l}2\left[\begin{array}{l}m_1A_2\left(\bar{h}^{4+n_\rho}-\bar{h}^{-m_1}\right)\bar{r}^{m_1} \\ +m_2A_3\left(\bar{h}^{4+n_\rho}-\bar{h}^{-m_2}\right)\bar{r}^{m_2}\end{array}\right] \\ \overline{h}^{-m_1}-\overline{h}^{-m_2} \\ +(3+n_\rho-n_E)\bar{r}^{(2-n_E+n_\rho)}\end{array}\right\}-\bar{r}^{n_\sigma} \tag{13}$$

Yielding occurs when above equation equals zero for the corresponding load parameters such as angular velocity ω, yield stress σ_0, and modulus of elasticity E. These parameters are rearranged and defined together as non-dimensional loading parameter (NLP):

$$NLP=\frac{\overline{\omega}}{\sqrt{\overline{\sigma}_0}} \tag{14}$$

NLP in the causes of which $\sigma_{\text{Tresca}} = 0$ is called the maximum angular velocity of the shaft. As it is shown in Fig. 4 considering variable modulus of elasticity, density, and yield stress may cause yielding starts from the inner, outer, or simultaneously from the inner and outer surfaces of the shaft. The plastic region grows through the radial direction by increasing the angular velocity of the shaft results in raising the plastic elastic region ratio. Hence, determining the effect of radius ratio on stress ordonnance and then resumption of

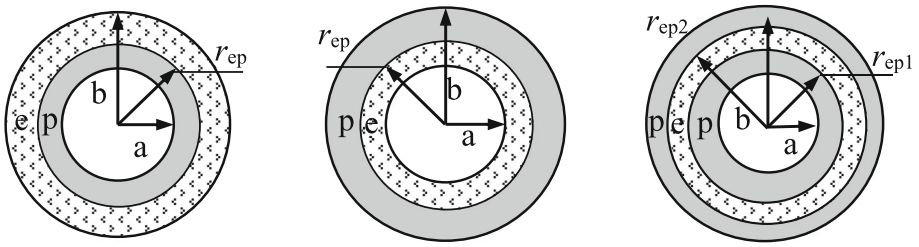

Fig. 2 Plastic deformations initiate from (**a**) the internal surface, (**b**) the outer surface of the rotor, and (**c**) both

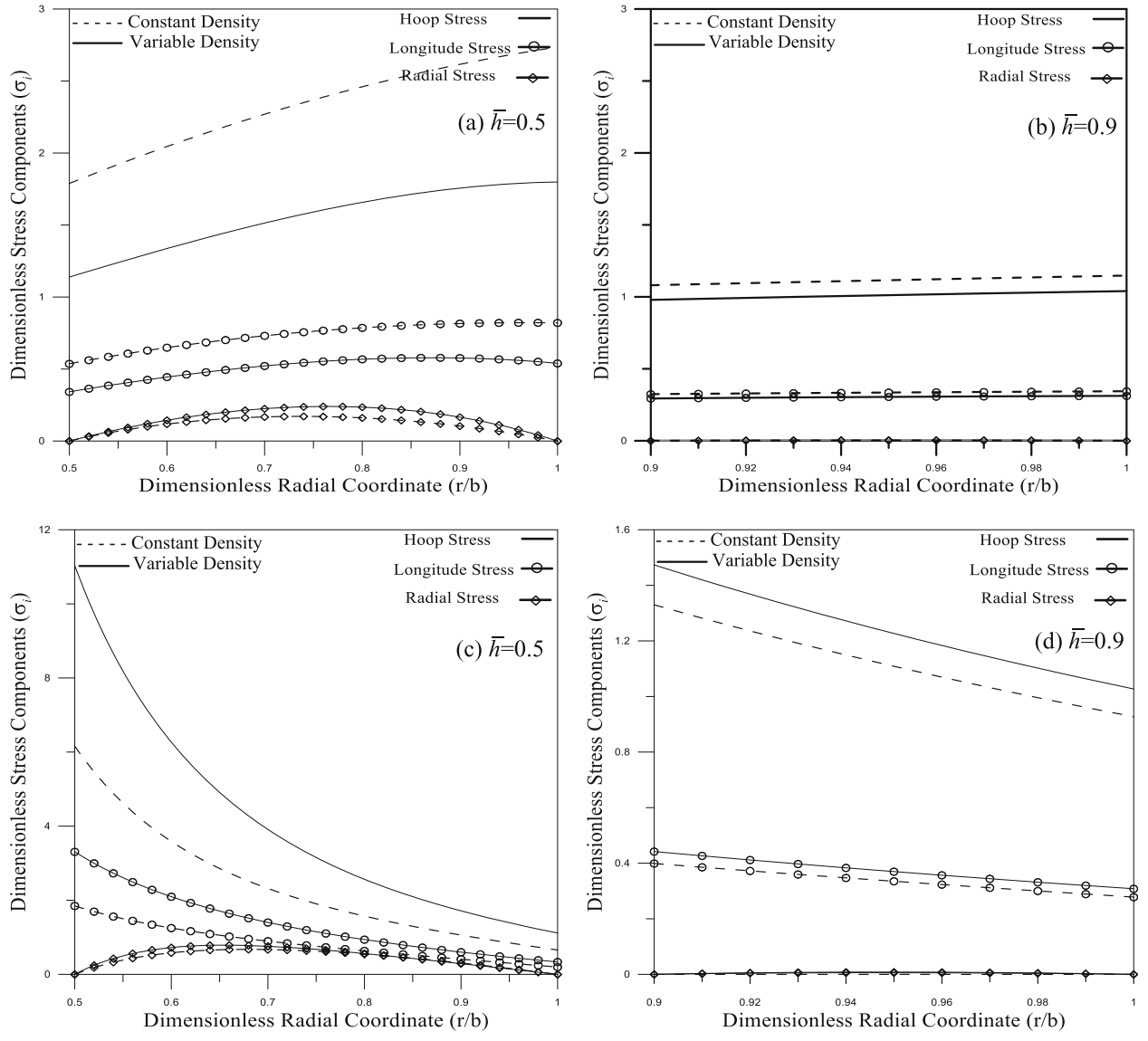

Fig. 3 Effect of density and radius ratio on stress collocation for $n_i = 2$ (**a**, **b**) and $n_i = -2$ (**c**, **d**)

yielding initiation for the remaining elastic region is needed. Equilibrium equation of rotating tube (2) is independent of the elastic-plastic behavior of the material. Using Tresca's yield criterion will give radial stress as follows:

$$\sigma_r = (\sigma_0/n)\bar{r}^n - \rho_0\bar{r}^m\left[r^2\omega^2/(m+2)\right] + C_3 \tag{15}$$

To verify different conditions, it is supposed that yielding will initiate from both surfaces of the tube. For the yielding initiation from the inner radius of the shaft, the proposed boundary condition to determine C_3 is ($\sigma_r(r=h) = 0$). Substituting C_3 into radial stress and using stress relations will result:

$$\begin{aligned}
\bar{\sigma}_{\bar{r}} &= \frac{\bar{\sigma}_0}{n_\sigma}\left(\bar{r}^{n_\sigma} - \bar{h}^{n_\sigma}\right) + \frac{\bar{\omega}^2}{n_\rho+2}\left(\bar{h}^{n_\rho+2} - \bar{r}^{n_\rho+2}\right)\\
\bar{\sigma}_\theta &= \frac{\bar{\sigma}_0}{n_\sigma}\left(\bar{r}^{n_\sigma}(1+n_\sigma) - \bar{h}^{n_\sigma}\right) + \frac{\bar{\omega}^2}{n_\rho+2}\left(\bar{h}^{n_\rho+2} - \bar{r}^{n_\rho+2}\right)\\
\bar{\sigma}_z &= \nu\left(\frac{\bar{\sigma}_0}{n_\sigma}\left(-2\bar{h}^{n_\sigma} + \bar{r}^{n_\sigma}(2+n_\sigma)\right) + \frac{2\bar{\omega}^2}{n_\rho+2}\left(\bar{h}^{n_\rho+2} - \bar{r}^{n_\rho+2}\right)\right)
\end{aligned} \tag{16}$$

Constants C_1 and C_2 related to the elastic region are obtained using stress continuity condition in different regions ($\sigma_r(r = r_{ep})_{\text{elastic}} = \sigma_r(r = r_{ep})_{\text{plastic}}$, $\sigma_r(r = 1)_{\text{elastic}} = 0$, r_{ep} is the elastic-plastic border of the shaft).

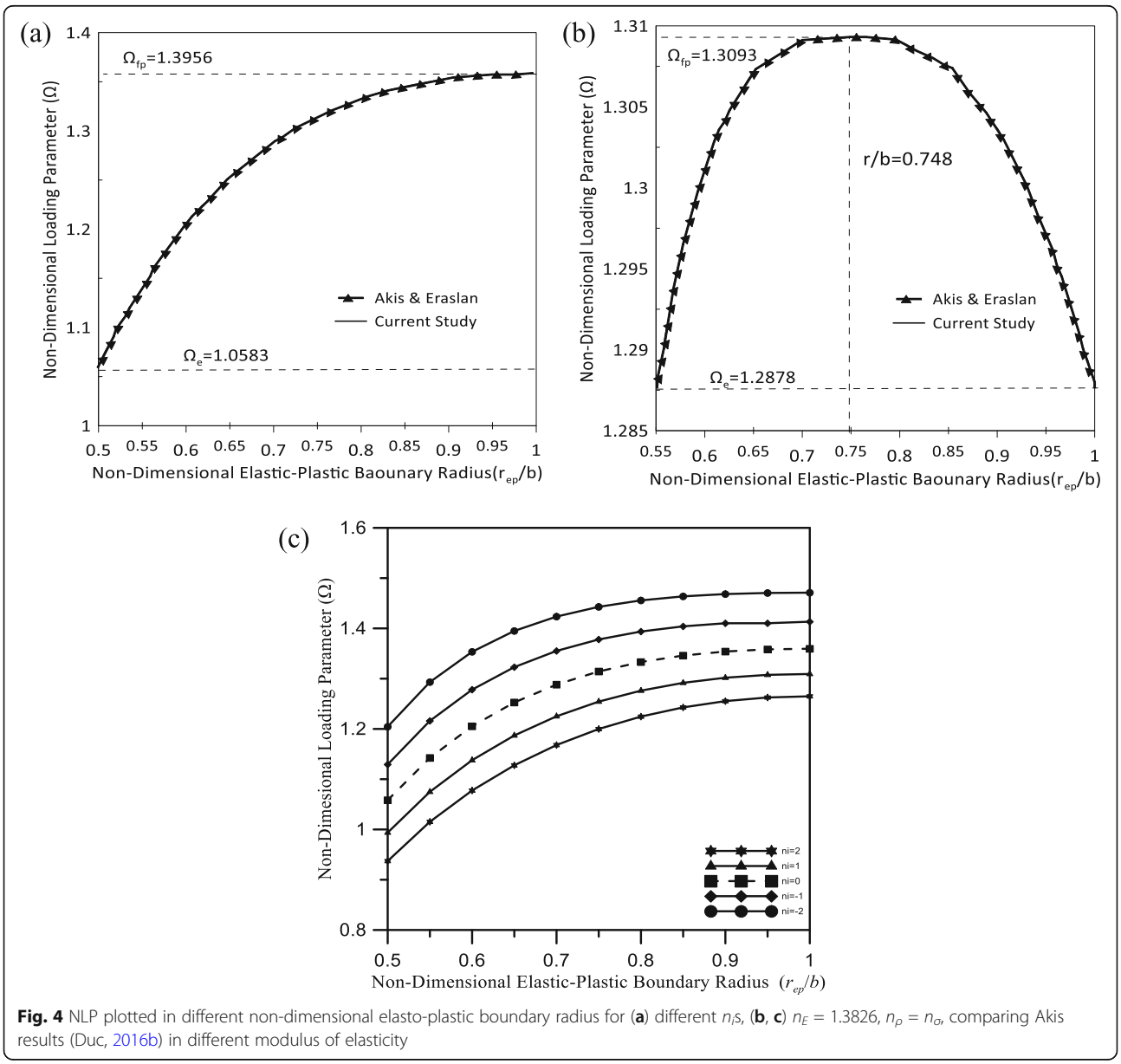

Fig. 4 NLP plotted in different non-dimensional elasto-plastic boundary radius for (**a**) different n_is, (**b**, **c**) $n_E = 1.3826$, $n_\rho = n_\sigma$, comparing Akis results (Duc, 2016b) in different modulus of elasticity

In the case of yielding initiation from the outer radius of the shaft, the following boundary condition is used to determine C_3 ($\sigma_r(r = 1) = 0$). The plastic stresses are:

$$\begin{aligned}
&\overline{\sigma}_r = \frac{\overline{\sigma}_0}{n_{\overline{\sigma}}}\left[\overline{r}^{n_\sigma}-1\right] + \frac{\overline{\omega}^2}{n_\rho+2}\left[1-\overline{r}^{n_{\rho+2}}\right] \\
&(n_i \to 0) \Rightarrow \overline{\sigma}_r = \left(\frac{\overline{\omega}^2}{2}\right)\left(1-\overline{r}^2\right) + \overline{\sigma}_0 \ln(r/a) \\
&\overline{\sigma}_\theta = \frac{\overline{\sigma}_0}{n_\sigma}\left(\overline{r}^{n_\sigma}(1+n_\sigma)-1\right) + \frac{\overline{\omega}^2}{n_\rho+2}\left(1-\overline{r}^{n_\rho+2}\right) \\
&(n_i \to 0) \Rightarrow \overline{\sigma}_\theta = \frac{\overline{\omega}^2}{2}\left(1-\overline{r}^2\right) + \overline{\sigma}_0 \ln(r/a) + \overline{\sigma}_0 \\
&\overline{\sigma}_z = \nu\left(\frac{\overline{\sigma}_0}{n_\sigma}\left(\overline{r}^{n_\sigma}(2+n_\sigma)-2\right) + \left[\frac{2\overline{\omega}^2}{n_\rho+2}\right]\left(1-\overline{r}^{n_{\rho+2}}\right)\right) \\
&(n_i \to 0) \Rightarrow \overline{\sigma}_z = \nu\left(\overline{\omega}^2\left(1^2-\overline{r}^2\right) + 2\overline{\sigma}_0 \ln(r/a)\right)
\end{aligned} \tag{17}$$

In the state of yielding initiation simultaneously from inner and outer radii of the shaft, the constants C_1 and C_2 related to radial elastic displacement and C_3 and C_4 related to radial plastic displacement and also r_{ep1} and r_{ep2} should be obtained simultaneously. Six equations are needed:

$$\begin{aligned}
&\overline{\sigma}_{\overline{r}}\Big|^{elastic}\left(\overline{r} = \overline{r}_{ep1}\right) = \overline{\sigma}_{\overline{r}}\Big|^{elastic}\left(\overline{r} = \overline{r}_{ep1}\right) \\
&\overline{u}\Big|^{elastic}\left(\overline{r} = \overline{r}_{ep1}\right) = \overline{u}\Big|^{plastic}\left(\overline{r} = \overline{r}_{ep1}\right) \\
&\overline{u}\Big|^{elastic}\left(\overline{r} = \overline{r}_{ep1}\right) = \overline{u}\Big|^{plastic}\left(\overline{r} = \overline{r}_{ep1}\right) \\
&\overline{\sigma}_{\overline{r}}\Big|^{elastic}\left(\overline{r} = \overline{r}_{ep2}\right) = \overline{\sigma}_{\overline{r}}\Big|^{elastic}\left(\overline{r} = \overline{r}_{ep2}\right) \\
&\overline{u}\Big|^{elastic}\left(\overline{r} = \overline{r}_{ep2}\right) = \overline{u}\Big|^{plastic}\left(\overline{r} = \overline{r}_{ep2}\right) \\
&\overline{\sigma}_\theta\Big|^{elastic}\left(\overline{r} = \overline{r}_{ep2}\right) - \overline{\sigma}_{\overline{r}}\Big|^{elastic}\left(\overline{r} = \overline{r}_{ep2}\right) = \overline{\sigma}_Y
\end{aligned} \tag{18}$$

Associated flow rule for this state of stress order (Akis & Eraslan, 2007) is $\varepsilon_\theta{}^p = -\varepsilon_r{}^p$ and $\varepsilon_z{}^p = 0$. Superscripts e and p refer to elastic and plastic states (Fig. 2).

$$\begin{aligned}
&\varepsilon^T = \varepsilon^p + \varepsilon^e \\
&\varepsilon^p = \varepsilon_r^p + \varepsilon_\theta^p + \varepsilon_z^p \\
&\varepsilon^e = \varepsilon_r^e + \varepsilon_\theta^p + \varepsilon_z^e
\end{aligned} \tag{19}$$

The associated flow rule expresses that the total plastic strain equals zero ($\varepsilon^p = 0$). Hence, total elastic and plastic strains are as follows:

$$\varepsilon^T = \varepsilon^p + \varepsilon^e = \varepsilon_r^e + \varepsilon_\theta^e = \frac{d\overline{u}}{d\overline{r}} + \frac{\overline{u}}{\overline{r}} \tag{20}$$

By knowing general stress-strain relations and using Hook's general law and Tresca's yield criterion, the stress-displacement equation becomes:

$$\begin{aligned}
&\varepsilon_{ij} = \frac{1}{E}\left(\sigma_{ij}-\nu\left(\sigma_{kk}-\sigma_{ij}\right)\right); \sigma ij = \frac{\partial u}{\partial \varepsilon_{ij}}; i,j,k = x,y,z \\
&\frac{d\overline{u}}{d\overline{r}} + \frac{\overline{u}}{\overline{r}} = \frac{1}{\overline{r}^{n_E}}\left(\left(1-\nu-\nu^2\right)\left(2\overline{\sigma}_r + \overline{\sigma}_Y\right)\right)
\end{aligned} \tag{21}$$

Substituting obtained plastic stresses into the above relation and rearranging it, we have:

$$\frac{d\overline{u}}{d\overline{r}} + \frac{\overline{u}}{\overline{r}} = \frac{2(1-\nu-2\nu^2)}{\overline{r}^{n_E}}\left\{\begin{array}{l}\frac{\overline{\sigma}_0}{n_\sigma}\left(\left(\frac{n_\sigma}{2}+1\right)\overline{r}^{n_\sigma}-\overline{h}^{n_\sigma}\right) \\ +\frac{\overline{\omega}^2}{n_\rho+2}\left(\overline{h}^{n_\rho+2}-\overline{r}^{n_\rho+2}\right)\end{array}\right\} \tag{22}$$

A non-dimensional solution of the above equation gives plastic radial displacement as follows:

$$\frac{u(r)}{r} = \frac{1-\nu-2\nu^2}{n_\rho+2} \times \left\{\begin{array}{l}\frac{-2\overline{r}^{-n_E}}{n_\sigma(-2+n_E)}\left(\sigma_0\overline{h}^{n_\sigma}(n_\rho+2)\right) - \frac{2\overline{\omega}^2\overline{r}^{-n_E+n_\rho+2}}{-4+n_E-n_\rho} \\ -\overline{\omega}^2 n_\sigma \overline{h}^{n_\rho+2} \\ +\frac{\overline{\sigma}_0\left(n_\sigma n_\rho+2n_\sigma+2n_\rho+4\right)\overline{r}^{-n_E+n_\sigma}}{n_\sigma(-2+n_E-n_\sigma)}\end{array}\right\} + \frac{C_4}{\overline{r}^2} \tag{23}$$

To obtain C_4, the continuity condition of radial displacement through the elastic and plastic border is considered.

$$u\Big|^{elastic}\left(\overline{r} = \overline{r}_{ep}\right) = u\Big|^{plastic}\left(\overline{r} = \overline{r}_{ep}\right) \tag{24}$$

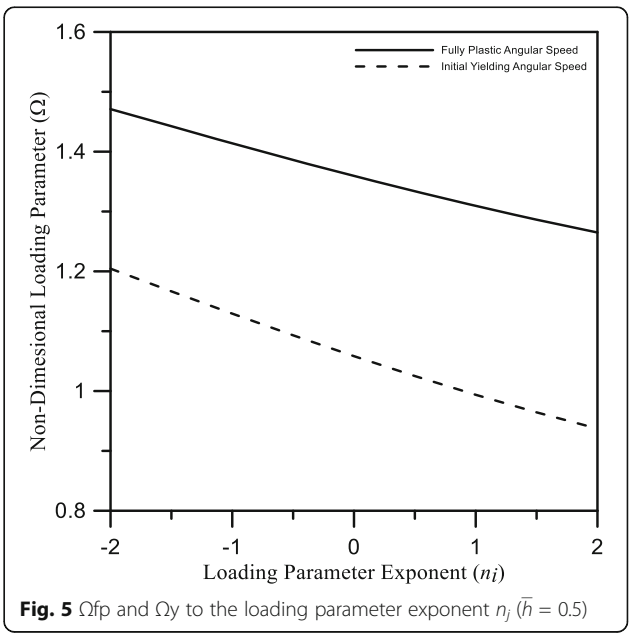

Fig. 5 Ωfp and Ωy to the loading parameter exponent n_j ($\overline{h} = 0.5$)

Results and discussion

Elastic results

Verification has been done by comparing results with articles discussed on homogenous materials and prior FGM articles which are shown on subsequent plots and considering modulus of elasticity as the only variable property of the material. $n_E = n_\rho = n_\sigma = 0$ (the homogenous material condition) for the limit of (21) and $n_i = 0$ creates:

$$\Omega = \overline{\omega}/\sqrt{\overline{\sigma}_0} = 2\left(\overline{h}\right)\sqrt{(1-\nu)/(1-2\nu) + (3-2\nu)\left(\overline{h}\right)^2} \quad (25)$$

The above equation is the maximum allowed angular velocity in a homogeneous tube (Nino et al., 1987). The results are discussed for $-2 \le n_i \le 2$ and $h = 0.5$ and $h = 0.55$ for $\nu = 0.3$ (Akis & Eraslan, 2007; Dai et al., 2006). To form Tresca's yield criterion, the stress collocation must be determined. Hoop, radial, and longitude stresses are plotted for different $h = a/b$ ratios and

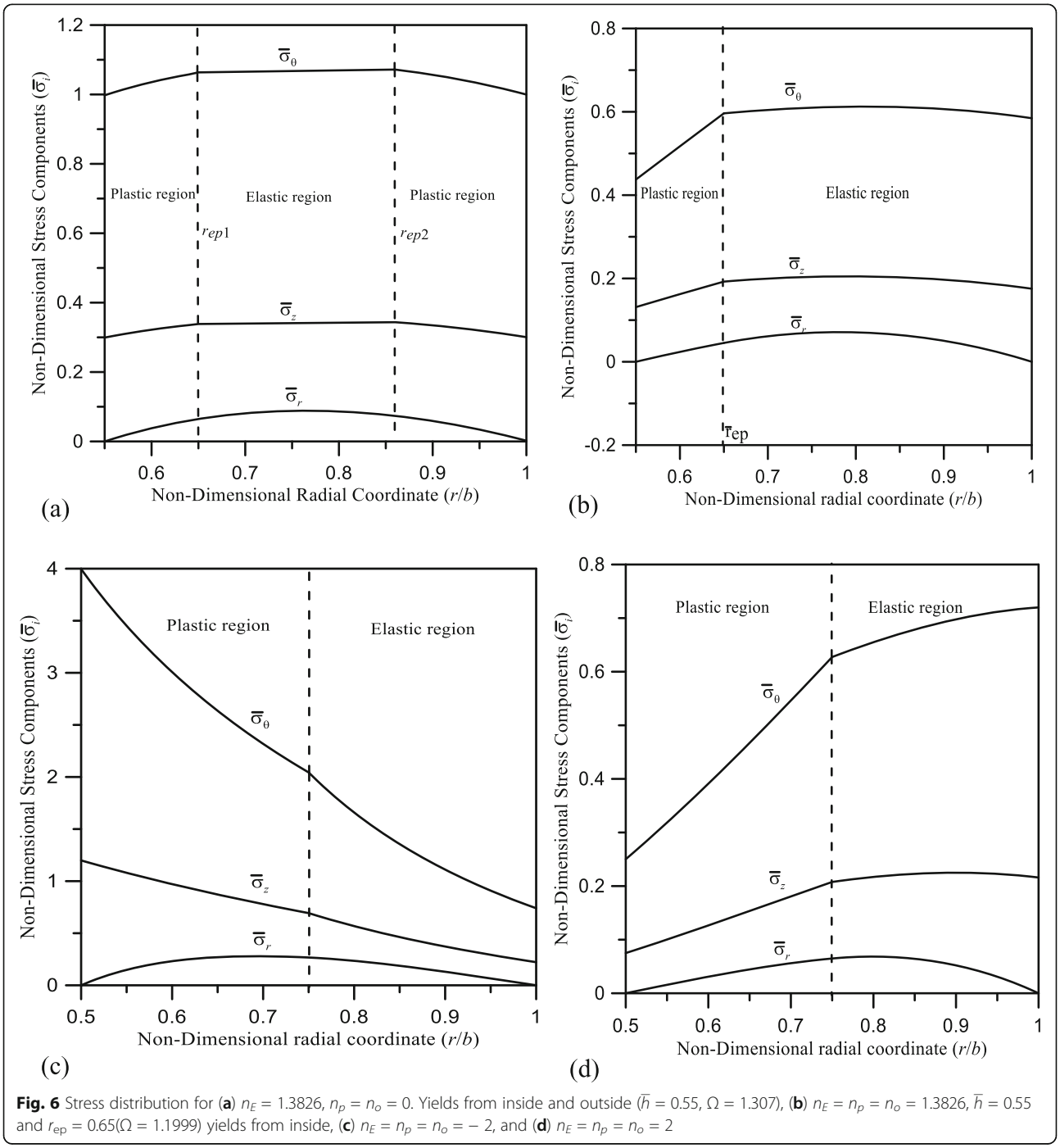

Fig. 6 Stress distribution for (**a**) $n_E = 1.3826$, $n_p = n_o = 0$. Yields from inside and outside ($\overline{h} = 0.55$, $\Omega = 1.307$), (**b**) $n_E = n_p = n_o = 1.3826$, $\overline{h} = 0.55$ and $r_{ep} = 0.65(\Omega = 1.1999)$ yields from inside, (**c**) $n_E = n_p = n_o = -2$, and (**d**) $n_E = n_p = n_o = 2$

different exponent parameters for both constant and variable density (Fig. 3).

When n_i = 2, the Hoop and longitude stress rising up for higher $r = r/b$, but radial stresses have a peak in the midrange of r. Hoop and longitude stresses have a higher value of dimensionless stress components for constant density in comparison with the variable density. Another fact is in $h > 0.9$ all studied stresses remain constant for different r. On the other hand, for $n_i = -2$, Hoop and longitude stresses descending, but there is no significant change in radial stress trends. The effects of the constant and variable density in values of dimensionless components are different and the higher values belong to variable density. These effects are identified in this study for the first time. Figure 3 reveals that the hoop stress is in maximum and radial stress is in the minimum value for $-2 \le n_i \le 2$ and $0.5 \le h \le 1$; hence, the Tresca's yield criterion is as defined before. Also, higher h ratios make the results more linear. In previous articles on the elastic-plastic behavior of FG rotating tube, the only variable of the material is defined as modulus of elasticity (Akis & Eraslan, 2007; Tsiatas & Babouskos, 2017). Circumferential stress has a smaller value when considering variable density. This trend is

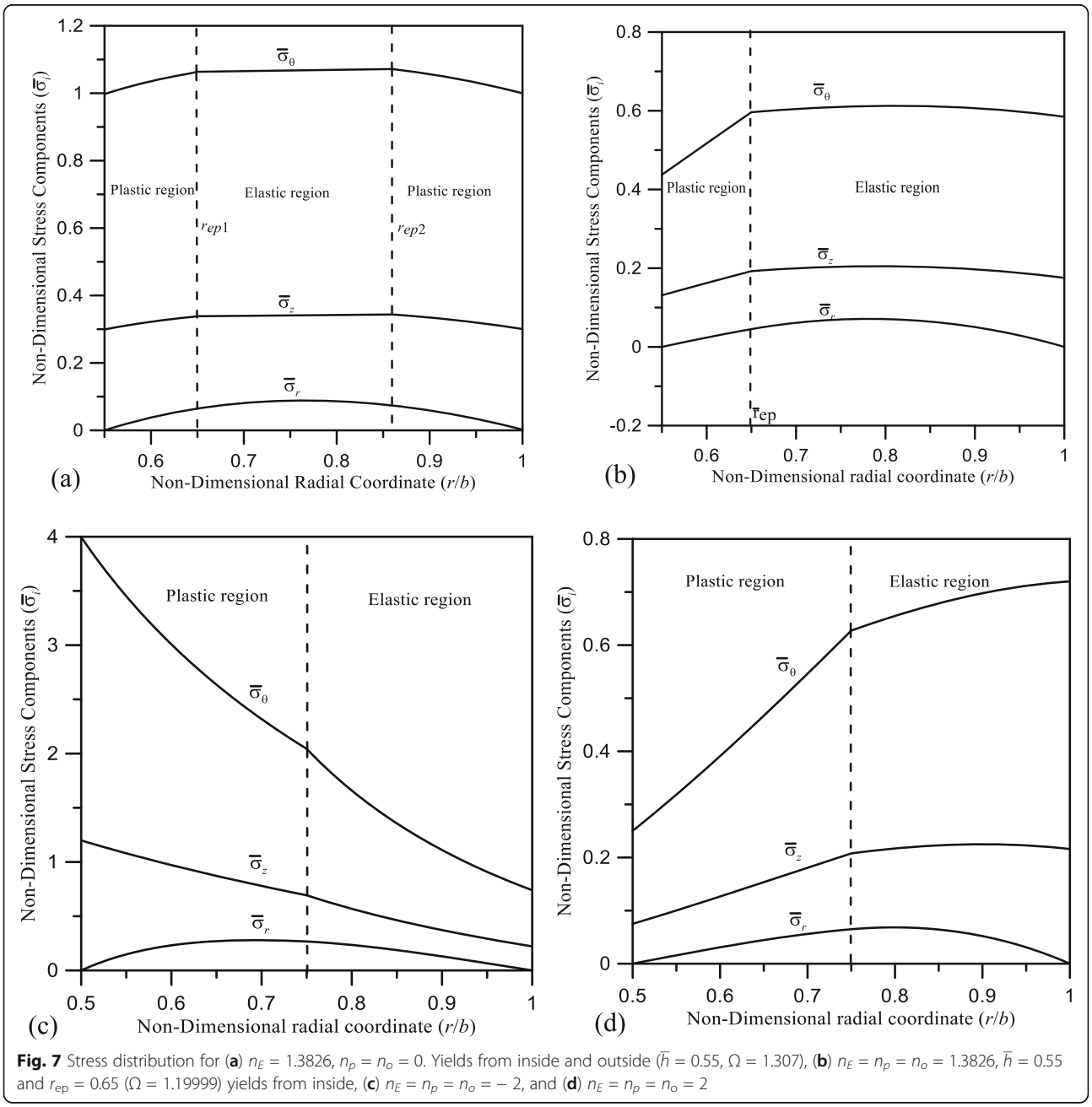

Fig. 7 Stress distribution for (**a**) n_E = 1.3826, $n_p = n_o = 0$. Yields from inside and outside ($\bar{h}$ = 0.55, Ω = 1.307), (**b**) $n_E = n_p = n_o$ = 1.3826, $\bar{h}$ = 0.55 and r_{ep} = 0.65 (Ω = 1.19999) yields from inside, (**c**) $n_E = n_p = n_o = -2$, and (**d**) $n_E = n_p = n_o = 2$

similar through a/b = 0.5 to 1 for n_i = 2, but these results are reverse for n_i = − 2. This phenomenon could be explained by considering power n_i. The power value sign is the reverse of material distribution through rotor wall thickness. For instance, when power law is a positive value, material distributed at outer radius of the rotor has greater density. So negative value of power will reverse material distribution which will result in different stress orders.

Plastic region

To validate the model for plastic deformations, a variable module of elasticity material (n_E = 1.3826, $n_\rho = n_\sigma$) considered to compare with (Akis & Eraslan, 2007). Figure 4a and b show that the results are the same for different NLP and r_{ep}/b. As Fig. 4a and b show, considering variable modulus of elasticity and constant density and yield stress limit may cause yielding initiation from an inner and outer radius of the shaft, simultaneously. High angular velocities create high centrifugal forces that made plastic deformations in the rotor. As shown in Fig. 4c, considering variable modulus of elasticity, density, and yield stress limit with the equal exponential rates will cause yielding from the inner radius of the shaft ($n_E = n_\rho = n_\sigma = n_i$ and $-2 \le n_i \le 2$). Also, the homogenous behavior of the rotating shaft is obtained ($n_E = n_\rho = n_\sigma = 0$). As it is depicted in Fig. 4c, higher plastic growth happened for higher NLPs and higher rotational speed as expected.

Plastic growth through radial coordinate by increasing the angular velocity of the shaft is shown in Fig. 5 for the different exponent of parameters. Maximum elastic and plastic velocity are also shown. In both, increasing n_i results in a reduction of non-dimensional loading parameter which causes yielding at lower speeds for the rotor. This is happening because of the lowering of the average of the material properties in higher exponential rates of material change. Neglecting yield and density changes make a considerable error not only in the calculation of non-dimensional loading parameters but also in the determination of yielding initiation point.

In Fig. 6, the elastic-plastic stresses are plotted for the state of plastic growth. To compare obtained results, plastic radial displacement is plotted for two conditions: considering variable modulus elasticity as the only variable of the material as Eraslan and Akis (Akis & Eraslan, 2007) (Fig. 6a) and considering variable modulus of elasticity, density, and yield stress limit as discussed above (Fig. 6b–d). Radial and hoop strains are plotted to verify and compare results. The plotted results are similar to the results from reference (Akis & Eraslan, 2007). According to Fig. 6, considering variable density and yield stress will change elastic-plastic radial displacement significantly. Similar to Fig. 3, the effects of the exponent rate are presented in Fig. 6c and d.

Plastic strains for the case of constant yield and density (Fig. 7a) and equal exponent rate for density, yield, and elastic modulus (Fig. 7b) investigated. The results are quite different in two cases for the equivalent non-dimensional loading parameter. Non-dimensional loading parameter (Ω) calculated as 1.307 according to Fig. 5 for fully plastic behavior (Fig. 7a) and 1.14 for a yield initiated case (Fig. 7b). The analogy between two cases again reveals that the yield initiates from inside if density, yield, and elastic modulus are variable. To have a better comparison, radial displacements for two cases (Fig. 7c and d) presented.

Finally, to get an analogy in different cases, the effect of variable density on radial displacement for a/b = 0.5 graphed in Fig. 8. It shows that for the same elastic modulus and yield stress exponent, lower density exponent reveals lower rotor displacement. Which is expected based on the authors' experience in different gas turbine rotor design and maintenance.

Conclusion

In the present article, elastic-plastic behavior of a rotating shaft made of FGM under high centrifugal forces is investigated for the first time. Modulus of elasticity, density, and yield stress is assumed to have a power-law function of the cylindrical coordinate system and all parameters concluded in an analytical model which is an improvement regarding previous jobs. The analytical equations derived based on different studies, and non-dimensional parameters defined to create comprehensive and analogical outcomes. The results are compared and validated with homogenous materials and previously published articles which

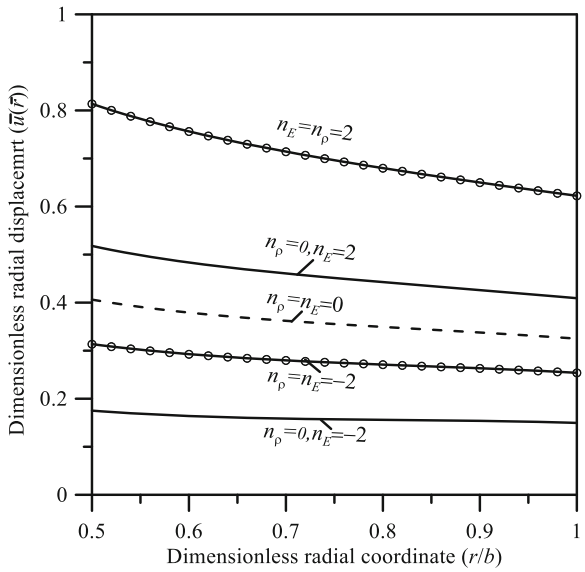

Fig. 8 Effect of variable density on radial displacement for a/b = 0.5

considered modulus of elasticity as the only variable of the material (Akis & Eraslan, 2007).

According to the presented research, the shaft's deformations and strength have a great dependency on the material property definition. The results show that neglecting the variety of density and yield stress causes a considerable difference in stress and strain and yielding initiation behavior may change from the inner surface of the shaft to its outer. It is essential to put great care to determine material properties for high-speed components such as hollow shaft to prevent design flaws in such sensible parts of the machine.

Due to the experience of the authors in gas turbine design industries, there is a need to have some robust formulas to check the yield point of hollow shafts during turbine maintenance. Different Rolls Royce gas turbine series such as Trent and AVON, Siemens SGT 800, and many other midsized turbines are using hollow shafts in their compressor and turbine parts. This model will help to control the yield start point for a hollow shaft measured during maintenance. This paper will pave a reliable way to design many high-speed rotary components. Although this research is about FGM materials, it could be outstretched for orthogonal and non-isotropic materials as well. The results will help designers to get a better perception of hollow shafts possible weaknesses and failures to design more efficient rotary machines.

Abbreviation
FGM: Functionally graded materials

Acknowledgements
The paper is theoretical work of the authors.

Authors' contributions
ST coordinated, validated, and formulated the data of the study. SA and MH contributed to literature review, calculations, and numerical analysis. All authors read and approved the final manuscript.

Funding
Not applicable

Availability of data and materials
Data are available by the request.

Ethics approval and consent to participate
Not applicable

Consent for publication
Not applicable

Competing interests
The authors declare that they have no competing interests.

Author details
[1]Sharif University of Technology, Azadi St., Tehran, Iran. [2]Isfahan University of Technology, Daneshgah-e Sanati Hwy, Isfahan, Iran.

Received: 9 September 2019 Accepted: 12 November 2019
Published online: 16 December 2019

References
Akis, T. (2009). Elastoplastic analysis of FG spherical pressure vessels. *Computational Materials Science, 46*, 545–554. https://doi.org/10.1016/j.commatsci.2009.04.017.

Akis, T., & Eraslan, A. (2007). Exact solution of rotating FGM shaft problem in the elastoplastic state of stress. *Archive of Applied Mechanics, 77*, 745–765. https://doi.org/10.1007/s00419-007-0123-3.

AnsariSadrabadi, S., Rahimi, G., Citarella, R., ShahbaziKarami, J., Sepe, R., & Esposito, R. (2017). Analytical solutions for yield onset achievement in FGM thick walled cylindrical tubes undergoing thermomechanical loads. *Composites Part B: Engineering, 116*, 211–223. https://doi.org/10.1016/j.compositesb.2017.02.023.

Bahaadini, R., & Saidi, A. (2018). Stability analysis of thin-walled spinning reinforced pipes conveying fluid in thermal environment. *European Journal of Mechanics - A/Solids, 72*, 298–309. https://doi.org/10.1016/j.euromechsol.2018.05.015.

Bahaloo, H., Papadopolus, J., & Ghosha, R. (2016). Transverse vibration and stability of an FG rotating annular disk with a circumferential crack. *International Journal of Mechanical Sciences, 113*, 26–35. https://doi.org/10.1016/j.ijmecsci.2016.03.004.

Bose, T., & Rattan, M. (2018). Effect of thermal gradation on steady state creep of functionally graded rotating disc. *European Journal of Mechanics - A/Solids, 67*, 169–176. https://doi.org/10.1016/j.euromechsol.2017.09.014.

Bouderba, B., Houari, M., Tounsi, A., & Mahmoud, S. (2016). Thermal stability of FG sandwich plates using a simple shear deformation theory. *Structural Engineering & Mechanics, 58-3*, 397–422. https://doi.org/10.12989/sem.2016.58.3.397.

Burzyński, S., Chróścielewski, J., Daszkiewicz, K., & Witkowski, W. (2018). Elastoplastic nonlinear FEM analysis of FGM shells of Cosserat type. *Composites Part B: Engineering, 154*, 478–491. https://doi.org/10.1016/j.compositesb.2018.07.055.

J.Chakrabarty, "Theory of plasticity", 3rd ed. Elsevier Butterworth-Heinemann, 2006.

Dai, H., Fu, Y., & Dong, Z. (2006). Exact solutions for functionally graded pressure vessels in a uniform magnetic field. *International Journal of Solids and Structures, 43*, 5570–5580. https://doi.org/10.1016/j.ijsolstr.2005.08.019.

Dai, T., & Dai, H. L. (2017). Analysis of a rotating FGMEE circular disk with variable thickness under thermal environment. *Applied Mathematical Modelling, 45*, 900–924. https://doi.org/10.1016/j.apm.2017.01.007.

Duc, N. D. (2013). Nonlinear dynamic response of imperfect eccentrically stiffened FGM double curved shollow shells on elastic foundation. *Journal of Composite Structures, 102*, 306–314. https://doi.org/10.1016/j.compstruct.2012.11.017.

Duc, N. D. (2016a). Nonlinear thermal dynamic analysis of eccentrically stiffened S-FGM circular cylindrical shells surrounded on elastic foundations using the Reddy's third-order shear deformation shell theory. *Journal of European Journal of Mechanics - A/Solids, 58*, 10–30. https://doi.org/10.1016/j.euromechsol.2016.01.004.

Duc, N. D. (2016b). Nonlinear thermo-electro-mechanical dynamic response of shear deformable piezoelectric Sigmoid functionally graded sandwich circular cylindrical shells on elastic foundations. *Journal of Sandwich Structures and Materials, 20-3*, 351–378. https://doi.org/10.1177/1099636216653266.

Duc, N. D., Bich, D. H., & Cong, P. H. (2016). Nonlinear thermal dynamic response of shear deformable FGM plates on elastic foundations. *Journal of Thermal Stresses, 39-3*, 278–297. https://doi.org/10.1080/01495739.2015.1125194.

Duc, N. D., & Cong, P. H. (2018). Nonlinear dynamic response and vibration of sandwich composite plates with negative Poisson's ratio in auxetic honeycombs. *Journal of Sandwich Structures and Materials, 20-6*, 692–717. https://doi.org/10.1177/1099636216674729.

Duc, N. D., Cong, P. H., Anh, V. M., Quang, V. D., Phuong, T., Tuan, N. D., & Thinh, N. H. (2015). Mechanical and thermal stability of eccentrically stiffened functionally graded conical shell panels resting on elastic foundations and in thermal environment. *Journal of Composite Structures, 132*, 597–609. https://doi.org/10.1016/j.compstruct.2015.05.072.

Duc, N. D., Homayoun, H., Quan, T. Q., & Khoa, N. D. (2019). Free vibration and nonlinear dynamic response of imperfect nanocomposite FG-CNTRC double curved shollow shells in thermal environment. *European Journal of Mechanics - A/Solids, 75*, 355–366. https://doi.org/10.1016/j.euromechsol.2019.01.024.

Duc, N. D., Khoa, N. D., & Thiem, H. T. (2018). Nonlinear thermo-mechanical response of eccentrically stiffened Sigmoid FGM circular cylindrical shells

subjected to compressive and uniform radial loads using the Reddy's third-order shear deformation shell theory. *Journal of Mechanics of Advanced Materials and Structures, 25-13*, 1157–1167. https://doi.org/10.1080/15376494.2017.1341581.

Duc, N. D., Kim, S. E., & Chan, D. Q. (2018). Thermal buckling analysis of FGM sandwich truncated conical shells reinforced by FGM stiffeners resting on elastic foundations using FSDT. *Journal of Thermal Stresses, 41-3*, 331–365. https://doi.org/10.1080/01495739.2017.1398623.

Duc, N. D., Lee, J., Nguyen-Thoi, T., & Thang, P. T. (2017). Static response and free vibration of functionally graded carbon nanotube-reinforced composite rectangular plates resting on Winkler-Pasternak elastic foundations. *Journal of Aerospace Science and Technology, 68*, 391–402. https://doi.org/10.1016/j.ast.2017.05.032.

Duc, N. D., Nguyen, P. D., & Khoa, N. D. (2017). Nonlinear dynamic analysis and vibration of eccentrically stiffened S-FGM elliptical cylindrical shells surrounded on elastic foundations in thermal environments. *Journal of Thin Walled Structures, 117*, 178–189. https://doi.org/10.1016/j.tws.2017.04.013.

Duc, N. D., Thang, P., Dao, N., & Vantac, N. (2015). Nonlinear buckling of higher deformable S-FGM thick circular cylindrical shells with metal–ceramic–metal layers surrounded on elastic foundations in thermal environment. *Composite Structure, 121*, 134–141. https://doi.org/10.1016/j.compstruct.2014.11.009.

Duc, N. D., Thuy Anh, V. T., & Cong, P. H. (2014). Nonlinear axisymmetric response of FGM shollow spherical shells on elastic foundations under uniform external pressure and temperature. *Journal of European Journal of Mechanics - A/Solids, 45*, 80–89. https://doi.org/10.1016/j.euromechsol.2013.11.008.

ND Duc, N.Tuan, P.Tran, P.Cong, P.Nguyen, "Nonlinear stability of eccentrically stiffened S-FGM elliptical cylindrical shells in thermal environment", Thin-Walled Structures, 108(2016) p.p.280-290 https://doi.org/10.1016/j.tws.2016.08.025.

El-Haina, F., Bakora, A., Bousahla, A., Tounsi, A., & Mahmoud, S. (2017). A simple analytical approach for thermal buckling of thick functionally graded sandwich plates. *Structural Engineering Mechanics, 63-5*, 585–595. https://doi.org/10.12989/sem.2017.63.5.585.

Eraslan, A., & Akis, T. (2006a). Plane strain analytical solutions for a functionally graded elastic–plastic pressurized tube. *International Journal of Pressure Vessels and Piping, 83*, 635–644. https://doi.org/10.1016/j.ijpvp.2006.07.003.

Eraslan, A., & Akis, T. (2006b). On the plane strain and plane stress solutions of functionally graded rotating solid shaft and solid disk problems. *Acta Mechanica, 181*, 43–63. https://doi.org/10.1007/s00707-005-0276-5.

Eraslan, A., & Akis, T. (2006c). The stress response of partially plastic rotating FGM hollow shafts: Analytical treatment for axially constrained ends. *Mechanics Based Design of Structures and Machines, 34-3*, 241–260. https://doi.org/10.1080/15397730600779285.

F.Figueiredo, L.Borges, F.Rochinha, "Elastoplastic stress analysis of thick-walled FGM pipes" AIP Conference Proceedings(2008) p.p. 147-52. https://doi.org/10.1063/1.2896766

Fukui, Y., & Yamanaka, N. (1991). Elastic analysis for thick-walled tubes of functionally graded material subjected to internal pressure. *JSME International Journal, 35-4*, 379–385. https://doi.org/10.1299/jsmea1988.35.4_379.

HosseiniKordkheili, S., & Naghdabadi, R. (2006). Thermoelastic analysis of a functionally graded rotating disk. *Composite Structure, 79-4*, 508–516. https://doi.org/10.1016/j.compstruct.2006.02.010.

Jabbari, M., Sohrabpour, S., & Eslami, M. (2002). Mechanical and thermal stresses in a functionally graded hollow cylinder due to radially symmetric loads. *International Journal of Pressure Vessels & Piping, 79-7*, 493–497. https://doi.org/10.1016/S0308-0161(02)00043-1.

Kargarnovin, M., Faghidian, S., & Arghavani, J. (2007). Limit analysis of FGM circular plates subjected to arbitrary rotational symmetric loads. *World Academy of Science, Engineering and Technology, 36*. https://doi.org/10.5281/zenodo.1332230.

Kaviprakash, G., Kannan, C., Lawrence, I., & Regan, A. (2014). Design and analysis of composite drive shaft for automotive application. *International Journal of Engineering Research & Technology, 3*, 429–436.

Khanna, K., Gupta, V., & Nigam, S. (2017). Creep analysis in functionally graded rotating disc using Tresca criterion and comparison with von-Mises criterion. *Materials Today Proceedings, 4-2-A*, 2431–2438. https://doi.org/10.1016/j.matpr.2017.02.094.

Khoa, N. D., Thiem, H. T., Thiem, o. T., & Duc, N. D. (2019). Nonlinear buckling and postbuckling of imperfect piezoelectric S-FGM circular cylindrical shells with metal-ceramic-metal layers in thermal environment using Reddy's third-order shear deformation shell theory. *Journal Mechanics of Advanced Materials and Structures, 26-3*, 248–259. https://doi.org/10.1080/15376494.2017.1341583.

Klocke, F., Klink, A., & Veselovac, D. (2014). Turbomachinery component manufacture by application of electrochemical, electro-physical and photonic processes. *CIRP Annals, 63-2*, 703–726 https://doi.org/10.1016/j.cirp.2014.05.004.

Lal, A., Jagtap, K., & Singh, B. (2013). Post buckling response of FGM plate subjected to mechanical and thermal loadings with random material properties. *Applied Mathematical Modelling, 37-5*, 2900–2920 https://doi.org/10.1016/j.apm.2012.06.013.

Lee, D., Kim, H., Kim, J., & Kim, J. (2004). Design and manufacture of an automotive hybrid aluminum composite drive shaft. *Composite Structures, 63*, 87–99. https://doi.org/10.1016/S0263-8223(03)00136-3.

Mack, W. (1991). Rotating elastic-plastic tube with free ends. *International Journal of Solids and Structures, 27*, 1462–1476. https://doi.org/10.1016/0020-7683(91)90042-E.

Mahamood, R., & Akinlabi, E. (2017). *"Functionally graded materials", Topics in Mining*. Springer, Switzerland: Metallurgy & Materials Eng.

Mathew, T., Natarajan, S., & Pañeda, E. (2018). Size effects in elastic-plastic functionally graded materials. *Composite Structures, 204*, 43–51. https://doi.org/10.1016/j.compstruct.2018.07.048.

Mendelson, A. (1968). *Plasticity, theory and application*. NewYork: Macmillman.

Moorthy, R., Mitiku, Y., & Sridhar, K. (2013). Design of automobile driveshaft using carbon/epoxy and kevlar/epoxy composites. *American Journal of Engineering Research, 2*, 173–179.

Nino, M., Hirai, T., & Watanabe, R. (1987). The functionally gradient materials. *Journal of Japan Society of Composite Material, 13*, 257–264.

Peng, X., & Li, X. (2012). Elastic analysis of rotating functionally graded polar orthotropic disks. *International Journal of Mechanical Sciences, 60*, 84–91. https://doi.org/10.1016/j.ijmecsci.2012.04.014.

Seraj, S., & Ganesan, R. (2018). Dynamic instability of rotating doubly-tapered laminated composite beams under periodic rotational speeds. *Composite Structures, 200*, 711–728. https://doi.org/10.1016/j.compstruct.2018.05.133.

Swaminathan, K., Naveenkumar, D., Zenkour, A., & Carrera, E. (2015). Stress, vibration and buckling analyses of FGM plates—A state-of-the-art review. *Composite Structures, 120*, 10–31. https://doi.org/10.1016/j.compstruct.2014.09.070.

Thom, D. V., Kien, N. D., Duc, N. D., Duc, D. H., & Tinh, B. Q. (2017). Analysis of bi-directional functionally graded plates by FEM and a new third-order shear deformation plate theory. *Journal of Thin Walled Structures, 119*, 687–699. https://doi.org/10.1016/j.tws.2017.07.022.

S. P. Timoshenko and J. N. Goodier, "Theory of elasticity", 3rd edition, McGraw-Hill, NY, 1970.

Torabnia, S., Hemati, M., & Aghajanib, S. (2019). Investigation of a hollow shaft to determine the maximum angular velocity regarding the FGM properties. *Materials Science Forum, 969*, 669–677 https://doi.org/10.4028/www.scientific.net/MSF.969.669.

Tsiatas, G., & Babouskos, N. (2017). Elastic-plastic analysis of functionally graded bars under torsional loading. *Composite Structures, 176*, 254–267. https://doi.org/10.1016/j.compstruct.2017.05.044.

Tutuncu, N., & Ozturk, M. (2001). Exact solutions for stress in functionally graded pressure vessels. *Composites Part B: Engineering, 32-8*, 683–686. https://doi.org/10.1016/S1359-8368(01)00041-5.

Yildirim, S., & Tutuncu, N. (2018). On the inertio-elastic instability of variable-thickness functionally-graded disks. *Mechanics Research Communications, 91*, 1–6. https://doi.org/10.1016/j.mechrescom.2018.04.011.

You, L., You, X., Zhang, J., & Li, J. (2007). On rotating circular disks with varying material properties. *Zeitschrift für angewandte Mathematik und Physik, 58*, 1068–1084. https://doi.org/10.1007/s00033-007-5094-2.

You, L., Zhang, J., & You, X. (2005). Elastic analysis of internally pressurized thick-walled spherical pressure vessels of functionally graded materials. *International Journal of Pressure Vessels and Piping, 82*, 347–354. https://doi.org/10.1016/j.ijpvp.2004.11.001.

ZamaniNejad, M., & Rahimi, G. (2010). Elastic analysis of FGM rotating cylindrical pressure vessels. *Journal of the Chinese Institute of Engineers, 33-4*, 525–530. https://doi.org/10.1080/02533839.2010.9671640.

Zharfi, H., & EkhteraeiToussi, H. (2018). Time dependent creep analysis in thick FGM rotating disk with two-dimensional pattern of heterogeneity. *International Journal of Mechanical Sciences, 140*, 351–360. https://doi.org/10.1016/j.ijmecsci.2018.03.010.

Publisher's Note